

# Effects of the body force on the pedestrian and the evacuation dynamics

I.M. Sticco<sup>a</sup>, G.A. Frank<sup>b</sup>, C.O. Dorso<sup>a,c,\*</sup>

<sup>a</sup>*Departamento de Física, Facultad de Ciencias Exactas y Naturales,  
Universidad de Buenos Aires,*

*Pabellón I, Ciudad Universitaria, 1428 Buenos Aires, Argentina.*

<sup>b</sup>*Unidad de Investigación y Desarrollo de las Ingenierías, Universidad Tecnológica  
Nacional, Facultad Regional Buenos Aires, Av. Medrano 951, 1179 Buenos Aires,  
Argentina.*

<sup>c</sup>*Instituto de Física de Buenos Aires,  
Pabellón I, Ciudad Universitaria, 1428 Buenos Aires, Argentina.*

---

## Abstract

The Social Force Model (SFM) is a suitable model for describing crowd behaviors under emotional stress. This research analyzes the role of the body force in the original SFM. We focused on the parameter associated with the body stiffness ( $k_n$ ) and its impact on the pedestrian dynamics for two different geometries: bottlenecks and corridors. Increasing  $k_n$  produces opposite effects on the crowd dynamics for each geometry: an increase of the crowd velocity for bottlenecks, and a decrease for corridors. The former reflects the fact that an increase in the stiffness reduces the overlap between pedestrians and, as a consequence, the sliding friction is diminished. This phenomenon reduces the number of blocking clusters close to the exit door. In the case of the corridor, instead, due to the confining walls, the pedestrians get tight into a lattice-like configuration due to space limitations. The friction interaction with the walls determines the velocity of the whole crowd along the corridor. Additionally, the corridor geometry generates a flux slowing down for very crowded environments, as observed in many real-life situations. We also explored the dimensionless parameters that arose from the reduced-in-units equation of motion and tuned them to reproduce the qualitative behavior of the empirical fundamental diagram.

---

\*codorso@df.uba.ar

*Keywords:*

Pedestrian Dynamics, Social Force Model, Body Force

*PACS:* 45.70.Vn, 89.65.Lm

---

## 1. Introduction

The Social Force Model (SFM) models the crowd dynamics considering three kinds of forces: desired forces, social forces, and physical forces. In its original version, the SFM, addresses two physical forces as essential: the “body force” and the “sliding friction”. Both are inspired by granular interactions and were claimed to be necessary for attaining the particular effects in panicking crowds [1]. The “sliding friction” actually proved to be an essential feature of the “faster-is-slower” effect, although the role of the “body force” appears, at a first instance, not so clear [2, 3, 4].

The existence of a “body force” in the context of highly dense crowds (say, more than 5 people/m<sup>2</sup>) is a commonsense matter [5, 6]. Researchers, however, question the numerical setting for this force in the SFM context [7]. As a matter of fact, the usual set of parameters provided by Helbing prevents the excessive overlapping among pedestrians, but it is known to accomplish artificially high force levels [1, 7, 8, 9]. The force estimates from the SFM appear to be remarkably higher with respect to the reported real life data (say, an order of magnitude). The crowd motion simulations, however, present realistic results [7, 8, 10]. The point seems to be that the SFM focuses on the “collective behavior” due to clogging, missing the “individualistic” perspective of single pedestrians or very small groups [1, 5, 11].

Many researchers realized that modifying the SFM may (partially) fix the misleading results. It was proposed that the pedestrians’ psychological force (say, the “social force”) should be suppressed in the context of highly dense crowds [12, 13, 14, 15], or smoothly quenched according to the crowd density [16]. The authors in Refs. [17, 18] further proposed a rigid body model in order to completely avoid the overlapping phenomenon. This perspective dismisses any connection to a “sliding friction”. Conversely, other authors tried to limit the pedestrians acceleration by introducing “static friction” between the pedestrians and the floor [19]. This kind of friction, however, reduces the effective willings of the pedestrians.

A unique (and universal) set of parameters appears not available yet to our knowledge. The reason is that different numerical sets of parameters can lead to the same crowd dynamics. Actually, only a small set of dimensionless “numbers” control the crowd dynamics [20]. These are similar to those encountered in other active matter systems (Péclet number, etc.) [21]. We may hypothesize that while the dimensionless parameters provide some kind of control on the collective behavior in crowds, only a few numerical set of parameters can attain an “individualistic” meaning.

The numerical parameters for the “faster is slower” effect presented by Helbing and co-workers appears to have some drawbacks Ref. [1, 10, 20]. Although a single parameter (say, the desired velocity  $v_d$ ) is numerically varied to explain the phenomenon, the researcher may loose sight of the dimensionless “numbers” that truly control the crowd dynamics. The set of parameters in Ref. [1] also misses the “faster is faster” effect reported to occur at very high pedestrian densities [10, 22]. Moreover, the empirical fundamental diagram raises as a point of reference for the SFM control parameters [23, 10].

The fundamental diagram exhibits the flux behavior for either low density crowds (with rare contacts between pedestrians) and highly dense crowds (dominated by two body interactions). In the second case, crowds experience a flux slowing down, but other behaviors are also possible [23, 24]. We may suspect that the modeling of the “flux slowing down” within the context of the SFM will require the proper setting of the (dimensionless) controlling parameters. This working hypothesis was already examined in Ref. [20], but the parameter exploration was limited to the sliding friction, disregarding the body force. In this paper, we widen the investigation on the set of parameters to include the one associated to the body force. We will explore the complex interplay between the body force and the sliding friction among pedestrians. Recall that the interplay dynamics is not directly controlled by the set of parameters, but through dimensionless “numbers”, where the model parameters appear mixed between each other. Thus, this step up offers a challenge to the “individualistic” meaning of the parameter’s set.

The paper is organized as follows. We first recall the available experimental values on the body force and the sliding friction (see Section 2). Secondly, we introduce the reduced-in-units SFM and the three dimensionless numbers that control the crowd dynamics (see Section 3). We present our numeri-

cal simulations in Section 5. For the sake of clarity, this Section is separated into three major parts: the bottleneck scenario, the corridor scenario and the comparison with empirical data in Sections: 5.1, 5.2 and 5.3, respectively. Section 6 opens a detailed discussion from results in Section 5 and resumes our main conclusions.

## 2. Experimental background

The complex behavior of pedestrians features either his (her) feelings and the environmental conditions. The former is expressed, for example, by his (her) moving “attitude” (say, relaxed, normal, aggressive, etc). The latter brings out the observed separation between pedestrians. Also, the “contacts” between individuals produce some kind of “unwanted” slowing down. All these observed patterns are commonly quantified in the literature into a set of characteristic parameters. It is worth mentioning that the empirical data reported in this Section corresponds to non-panicking situations in which pedestrians do not experience high anxiety levels (see below). The experimental meaning of these parameters is as follows.

- (i) The walking attitude of a pedestrian may appear somewhat “aggressive” if he (she) reacts actively to unexpected behaviors [7, 25]. The smaller the reaction time, the more aggressive observed posture. The associated parameter to this behavior is the relaxation or characteristic time  $\tau$  [26, 1].
- (ii) Despite the reactive attitude  $\tau$ , the pedestrian adopts a “free” (undisturbed) walking speed  $v_d$ . This speed expresses his (her) motivation or intention to reach a certain destination (as comfortable as possible). Observations commonly associate 0.6 m/s, 1 m/s or 1.5 m/s to relaxed, normal or nervous walking speeds, respectively [25, 1, 27]. Nevertheless, when pedestrians are in a panic situation, they may not reach the “free” walking speed, but,  $v_d$  may still be associated to his (her) motivation to get to a target position.
- (iii) The walking speed of pedestrians appears to be lower in a crowded walkway with respect to their usually expected “free” walking speeds [28, 7]. Pedestrians tend to reduce their speed within crowded environments because they perceive not enough space for taking a step [26].

$\tau$ [s]	$m$ [kg]	$v_d$ [m/s]	$B$ [m]	$k_n$ [kg/s <sup>2</sup> ]	Refs.
0.61	—	1.24	$0.36 + 1.06 v$	—	[30]
0.50*	80*	1.34	0.50	—	[28, 7]
—	67.5	1.39	—	$96.1 + 12694.1 x$	[16]
—	67.0	1.39	—	$97.0 + 29378.9 x$	[16]

Table 1: The experimental data for the pedestrian parameters, as explained in Section 2. The magnitude  $v$  means the actual pedestrian velocity (m/s). The magnitude  $x$  means the compression length (m). The upper row for Ref. [16] corresponds to data acquired in winter and the lower row to data acquired in summer. The asterisk (\*) corresponds to reasonable estimates from the authors.

This (perceived) step distance is therefore an influential parameter on the pedestrians behavior. It is known as the characteristic length  $B$ .

- (iv) Physical interactions occur in very crowded environments. The “body force” and “sliding friction” can be introduced straight forward. This will be done in Section 3. But it is worth noting that both are associated to the moving difficulties (say, slowing down and obstructions) observed in contacting pedestrians.

Table 1 shows a few empirical values for the most common parameters. More data is available throughout the literature (see, for example, Refs. [29, 30, 31, 32, 33, 34, 27] ). We intentionally omitted data that assumes a specific mathematical model. The exhibited values should also be considered as a general purpose approach, since no distinction has been made on age, gender or cultural habits.

A first examination of the figures in Table 1 shows that the choice  $\tau \simeq 0.6$  s seems to be a reasonable estimation for the relaxation time, although this may vary with respect to gender or culture [35]. Additionally, we confirm that normal pedestrians attain desired velocities around 1.3 m/s.

The reports from Refs. [30, 28] do not include any values for the compressibility  $k_n$  since these experiments were carried out under low density and non-panicking conditions. The minimum (perceived) step distance is 0.36 m according to Ref. [30], but the pedestrians seem to require larger distances when they walk faster. The commonly accepted value  $B \simeq 0.5$  m is somewhat valid for walking speeds under 0.5 m/s and non-panicking conditions

[30]. Higher walking speeds (say, 1 m/s) will require a step distance of 1.3 m for the pedestrians to feel that there is enough space to move along.

The reported data from Ref. [16] correspond to the crowded environment of the Beijing subway. This environment was not suitable for providing information on the step distance  $B$ , but estimates for the desired speed and the body compressibility could be achieved. The reported magnitude  $k_n$  assesses either the clothes and the body compressibility. The final value, though, is linearly related to the compression (overlap)  $x$ .

We measured contact forces during the spring of 2019 at the subway in Buenos Aires, Argentina. Our preliminary results show that pedestrians feel “uncomfortable” whenever a body force ranging from 5 to 20 N is applied for at least ten minutes. Short lasting forces (say, less than 4 minutes) may also be perceived as “uncomfortable” for values ranging from 10 to 30 N. We also recorded body forces up to 60 N during very short “hits”. The comparison with the fittings provided by Ref. [16] shows that these magnitudes accomplish densities around 5 people/m<sup>2</sup>.

The maximum (realistic) overlap may be computed from the Hooke’s relation  $F(x) = k_n(x)x$  and the compressibility  $k_n(x)$  reported in Table 1. An “uncomfortable” body force 10 N – 30 N can address overlap values in the range of 0.030 – 0.055 m. Also, a “hitting” force of 60 N can address overlap values between 0.045 and 0.065 m. Besides, no reliable values for the sliding friction  $k_t$  appears to be available in the literature (to our knowledge).

### 3. Theoretical background

#### 3.1. The Social Force Model

The Social Force Model (SFM) provides a necessary framework for simulating the collective dynamics of pedestrians (*i.e.* self-driven particles). The pedestrians are considered to follow an equation of motion involving either “socio-psychological” forces and physical forces (say, granular forces). The equation of motion for any pedestrian  $i$  (of mass  $m_i$ ) reads

$$m_i \frac{d\mathbf{v}_i}{dt} = \mathbf{f}_d^{(i)} + \sum_{j=1}^N \mathbf{f}_s^{(ij)} + \sum_{j=1}^N \mathbf{f}_g^{(ij)} \quad (1)$$

where the subscript  $j$  corresponds to any neighboring pedestrian or the walls. The three forces  $\mathbf{f}_d$ ,  $\mathbf{f}_s$  and  $\mathbf{f}_g$  are different in nature. The desire force  $\mathbf{f}_d$  represents the acceleration (or deceleration) of the pedestrian due to his (her) own will. The social force  $\mathbf{f}_s$ , instead, describes the tendency of the pedestrians to stay away from each other. The granular force  $\mathbf{f}_g$  stands for both the sliding friction and the compression between pedestrians.

Notice that these forces are supposed to influence the behavior of the pedestrians in a similar fashion as mentioned in Section 2. Thus, the set of (empirical) parameters described in Section 2 is expected to be also present in the SFM. These will appear in connection to the forces.

The pedestrians' own will is modeled by the desire force  $\mathbf{f}_d$ . This force stands for the acceleration (deceleration) required to move at the desired walking speed  $v_d$ . This involves, however, a personal attitude that makes him (her) appear more or less "assertive". As mentioned in Section 2, the reaction time  $\tau$  reflects this attitude. Thus, the desire force is modeled as follows

$$\mathbf{f}_d^{(i)} = m \frac{v_d^{(i)} \hat{\mathbf{e}}_d^{(i)}(t) - \mathbf{v}^{(i)}(t)}{\tau} \quad (2)$$

where  $\hat{\mathbf{e}}(t)$  represents the unit vector pointing to the target position.  $\mathbf{v}(t)$  stands for the pedestrian velocity at time  $t$ .

The tendency of any individual to preserve his (her) "private sphere" is accomplished by the social force  $\mathbf{f}_s$ . This force is expected to prevent the pedestrians from getting too close to each other (or to the walls) in a any environment. The model for this kind of "socio-psychological" behavior is as follows

$$\mathbf{f}_s^{(i)} = A e^{(R_{ij}-r_{ij})/B} \hat{\mathbf{n}}_{ij} \quad (3)$$

where  $r_{ij}$  means the distance between the center of mass of the pedestrians  $i$  and  $j$ , and  $R_{ij} = R_i + R_j$  is the sum of the pedestrians radius. The unit vector  $\hat{\mathbf{n}}_{ij}$  points from pedestrian  $j$  to pedestrian  $i$ , meaning a repulsive interaction.

The net distance (overlap)  $|R_{ij} - r_{ij}|$  scales to the parameter  $B$  in the expression (3). This parameter plays the role of a fall-off length within the model, and thus, it may be somewhat connected to the (perceived) step distance mentioned in Section 2. Besides, the parameter  $A$  reflects the intensity of the social repulsion.

The granular force (say, the sliding friction plus the body force) reflects the moving difficulties encountered in very crowded environments. The expression for the granular force has been borrowed from the granular matter field, the mathematical expression reads as follows

$$\mathbf{f}_g^{(ij)} = k_t g(R_{ij} - r_{ij}) (\Delta \mathbf{v}^{(ij)} \cdot \hat{\mathbf{t}}_{ij}) \hat{\mathbf{t}}_{ij} + k_n g(R_{ij} - r_{ij}) \hat{\mathbf{n}}_{ij} \quad (4)$$

where  $g(R_{ij} - r_{ij})$  equals  $R_{ij} - r_{ij}$  if  $R_{ij} > r_{ij}$  and vanished otherwise.  $\Delta \mathbf{v}^{(ij)} \cdot \hat{\mathbf{t}}_{ij}$  represents the relative tangential velocities of the sliding bodies (or between the individual and the walls).

The sliding friction occurs in the tangential direction while the body force occurs in the normal direction. Both are assumed to be linear with respect to the net distance between contacting pedestrians. The sliding friction is also linearly related to the difference between the (tangential) velocities. The coefficients  $k_t$  (for the sliding friction) and  $k_n$  (for the body force) are supposed to be related to the areas of contact and the clothes material, among others.

We stress that the expression (4) assumes fixed values for  $k_t$  (and  $k_n$ ). This may not be completely true according to Table 1. The local density (and thus, the pedestrians' compression) may affect the compressibility parameter  $k_n$  by more than an order of magnitude. We will vary  $k_n$  (and  $k_t$ ) in order to explore this phenomenon.

### 3.2. The set of parameters

The numerical set of parameters may affect the dynamics of the pedestrians. Some values, however, yield similar collective dynamics. We introduce dimensionless magnitudes and proceed straightforward as indicated in Appendix A. We realize from Appendix A that only three (dimensionless) parameters are the true “control” parameters for the collective dynamics. These are  $\mathcal{A}$ ,  $\mathcal{K}$ ,  $\mathcal{K}_c$  as defined in Appendix A. Recall that  $\mathcal{A}$  and  $\mathcal{K}$  are precisely the same as in Ref. [20], but a novel  $\mathcal{K}_c$  parameter has been introduced



due to the body force.

The logical relations between the dimensionless parameters and the “individual” parameters can be studied by means of the Venn diagrams exhibited in Fig. 1. The parameters  $\mathcal{A}$ ,  $\mathcal{K}$  and  $\mathcal{K}_c$  are represented as intersecting sets, and the “individual” parameters are represented as elements within each set. The shared elements between  $\mathcal{A}$ ,  $\mathcal{K}$  and  $\mathcal{K}_c$  are placed inside the intersecting regions.

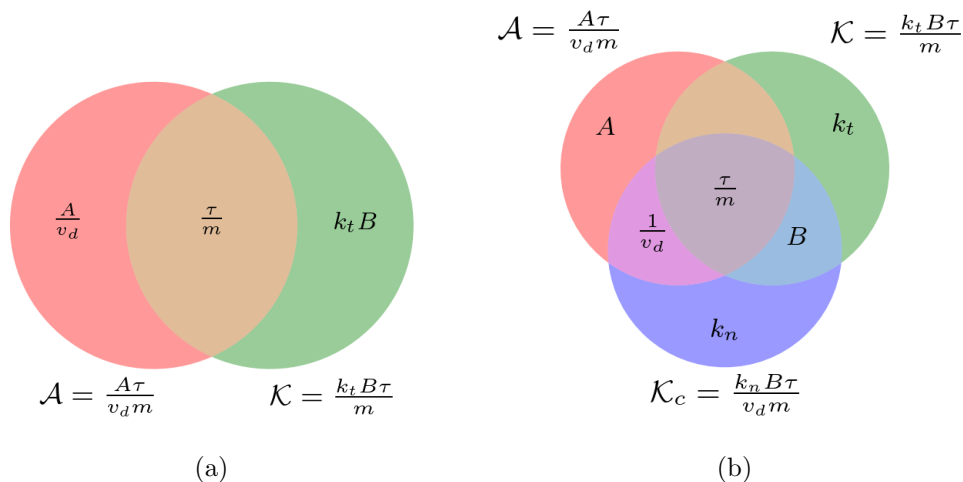


Figure 1: Venn diagrams for the dimensionless parameters appearing in the equation of motion (1) (see Appendix Appendix A for details). The sets correspond to  $\mathcal{A} = \{\tau/m, 1/v_d, A\}$ ,  $\mathcal{K} = \{\tau/m, B, k_t\}$  and  $\mathcal{K}_c = \{\tau/m, 1/v_d, B, k_n\}$ . (a) The Venn diagram representation if no body force is introduced in the SFM (only sets  $\mathcal{A}$  and  $\mathcal{K}$ , as in Ref. [20]). (b) The Venn diagram representation for the sets  $\mathcal{A}$ ,  $\mathcal{K}$  and  $\mathcal{K}_c$ .

A first inspection of the diagrams in Fig. 1 shows that the relaxation time (per unit mass)  $\tau/m$  is always a common parameter to all sets, regardless of the body force. This means that the “assertive” attitude of the pedestrian, addressed by the reaction time (see Section 2), applies to all stimuli and the own willings. The role of  $\tau$  has already been discussed in Refs. [26, 20].

Fig. 1a represents the situation when  $\mathcal{K}_c$  is absent. Notice that  $A/v_d$  or  $k_t B$  may control the collective dynamic, in spite of the “assertive” attitude. The individual character of  $v_d$  or  $B$  appears somehow “loosely” in the crowd

dynamic. We mean by “loosely” that any numerical set for these parameters may be counterbalanced by the right choice of  $A$  or  $k_t$ , keeping the collective dynamic (qualitatively) unchanged.

Fig. 1b provides a picture of the parameters’ relations after introducing  $\mathcal{K}_c$ . Surprisingly,  $\mathcal{K}_c$  appears as a wider set (say, a four elements set) than  $\mathcal{A}$  or  $\mathcal{K}$  (three elements’ sets). It shares the parameter  $v_d$  with  $\mathcal{A}$  and the parameter  $B$  with  $\mathcal{K}$ . The practical consequence to these (logical) relations is that  $v_d$  or  $B$  affect simultaneously two “control” parameters of the collective dynamics. Conversely, either  $v_d$  and  $B$  may counterbalance  $\mathcal{K}_c$  in order to keep the collective dynamic (qualitatively) unchanged.

We confirm from these diagrams that no univocal relations can be established between the individual parameters and the collective dynamics (in a crowded environment). The presence of the body force moves the dynamics to a more complex context. We will investigate this context in Section 5.

### 3.3. Blocking clusters

A characteristic feature of pedestrian dynamics is the formation of clusters. Clusters of pedestrians can be defined as the set of individuals that for any member of the group (say,  $i$ ) there exists at least another member belonging to the same group ( $j$ ) in contact with the former. Thus, we define a “granular cluster” ( $C_g$ ) following the mathematical formula given in Ref. [40]

$$C_g : P_i \in C_g \Leftrightarrow \exists j \in C_g / r_{ij} < (R_i + R_j) \quad (5)$$

where ( $P_i$ ) indicate the  $i$ th pedestrian and  $R_i$  is his (her) radius (shoulder width). That means,  $C_g$  is a set of pedestrians that interact not only with the social force, but also with physical forces (*i.e.* friction force and body force). A “blocking cluster” is defined as the subset of clusterized particles (granular cluster) closest to the door whose first and last component particles are in contact with the walls at both sides of the door [2]. This clogging structure is responsible for worsening the evacuation performance.

## 4. Working hypotheses and procedures

### 4.1. Working hypotheses

Our working hypotheses are similar to those mentioned in Ref. [20], although the presence of the body force opens inquiries about the proper exploration of the parameter space. To be precise

- (a) The “faster-is-slower” (or the “faster-is-faster”) phenomenon occurs when varying the values of  $v_d$  (see Section 5.1). This is equivalent to vary simultaneously  $\mathcal{A}$  and  $\mathcal{K}_c$  by the same amount in the (dimensionless) parameter space (see Section 3.2). We may visualize this sampling procedure as moving along a straight line in the space  $(\mathcal{A}, \mathcal{K}, \mathcal{K}_c)$ . Further variations of  $k_n$  turns the sample points out of this line, but on the plane of constant  $\mathcal{K}_c$ . We will step up  $k_n$  by several orders of magnitude in order to get the big picture of this surface.
- (b) We will consider the parameter set from Ref. [1] as a starting point for exploring the parameter space. The reason for this is that a complete set of experimental parameters is still not available (to our knowledge). We are aware, though, of the drawbacks of this choice, say, the unrealistic meanings for the length  $B$  and the compressibility  $k_n$  (see Section 2). But these are irrelevant in the context of the (dimensionless) parameter space and the corresponding collective dynamics (see Section 1).
- (c) We will explore crowd densities allowing body compressions (overlaps) up to 0.1 m. This corresponds to remarkably high densities, since our own (real-life) estimates do not surpass 0.065 m (see Section 2). Therefore, the extremely high density scenarios (say, above 0.065 m) will be considered for the purpose of a tendency, but not as a common real-life situation. No casualties due to high pressures will be further considered.

We stress the fact that our concern is placed on the collective dynamics of crowded environments. We will work on the hypothesis that any “reasonable” parameter set should reproduce the collective behavior (say, the slowing down in the fundamental diagram; see Section 5.3). We will not attempt to optimize parameters from other objective functions.

We will further sustain the hypothesis of soft matter in the context of crowded environments. The body compression and the sliding friction parameters are supposed to be connected in some way under this hypothesis. However, we will not introduce any direct link between  $\mathcal{K}$  and  $\mathcal{K}_c$ . We will investigate the interplay between both in Section 5.3.

In order to keep the model as simple as possible, we will only consider isotropic pedestrian interactions, since anisotropic interactions do not play a relevant role at high densities.

#### 4.2. Procedures

The SFM was implemented on the LAMMPS simulation software [39]. Additional modules for LAMMPS were also written in C++ in order to expand the software capabilities. All these were able to run in a high performance environment (HPC).

The implemented SFM parameters were the same as those in Ref. [1] (at the beginning of the exploratory procedure only). But the pedestrian's mass and radius were set to the more realistic values of 70 kg and 0.23 m, respectively. The force interactions between pedestrians were limited, however, to a cut-off distance of 0.88 m for attaining a *privacy sphere* that excludes second neighbors. The desired velocity was always set to 1 m/s in the corridor situation. Besides, the explored values of  $v_d$  for the bottleneck scenario ranged from 1 m/s to the extremely anxious situation of 10 m/s.

The Eq. (1) was numerically integrated by means of the velocity Verlet algorithm, with a timestep of  $10^{-4}$  seconds. The pedestrians positions and velocities were recorded every 0.05 sec, but post-processing computing was done over samples acquired at least every 2 sec., in order to avoid data correlations. Those pedestrians leaving the simulations box were re-introduced into the box, on the opposite side (periodic boundary conditions). We only omitted this mechanism when computing the evacuation time for the bottleneck geometry.

The post-processing computing was assisted by Python functions. The NetworkX package was used among others.

We warn the reader that, for simplicity, we will not include the units corresponding to the numerical results. Remember that the friction coefficient has units  $[k_t] = \text{Kg m}^{-1} \text{s}^{-1}$ , the body stiffness coefficient  $[k_n] = \text{Kg s}^{-2}$ , the density  $[\rho] = \text{p m}^{-2}$  and the flow  $[J] = \text{p m}^{-1} \text{s}^{-1}$ .

## 5. Results

### 5.1. Bottleneck

We present in this section the results corresponding to the bottleneck geometry. We show the consequences of modifying the body force coefficient  $k_n$  on the evacuation dynamics. Recall that this coefficient is associated to the compression of the human body.

Fig. 2 shows the evacuation time as a function of the pedestrian’s desired velocity for different values of  $k_n$ . The evacuation time is defined as the time lapsed until 80% of the pedestrians have left the room. In this section we will focus on the evacuation time for  $2 \text{ m/s} < v_d < 10 \text{ m/s}$ .

Three behavioral patterns can be distinguished in Fig. 2. Each pattern can display a positive slope, a negative slope or both. The interval in which the slope is positive means that the harder the pedestrians try to get out (higher  $v_d$ ), the longer it takes them to evacuate. This is the Faster-is-slower (FIS) regime. Conversely, the interval in which the slope is negative corresponds to a Faster-is-Faster (FIF) regime (the harder they try, the quicker they leave).

Fig. 2 shows either FIS or FIF, and a FIS+FIF pattern for desired velocities  $v_d > 1.2 \text{ m/s}$ . The evacuation time attains a FIS+FIF pattern for compression coefficients below  $k_n = 1.2 \text{ E}5$ . This means that “soft” individuals can attain this behavioral pattern. Notice that higher values of  $k_n$  allow only FIS or FIF patterns. For the highest explored value  $k_n = 1.2 \text{ E}6$ , no FIS can be seen at all. Besides, the evacuation pattern for  $k_n = 0$  and  $k_n = 2.6 \text{ E}4$  are very similar since the body force intensity is of the same order or less than the social force for these stiffness values.

Despite the presence of the FIS or FIF pattern, the evacuation time at a fixed value of  $v_d$  decreases for increasing values of  $k_n$  (within the exam-

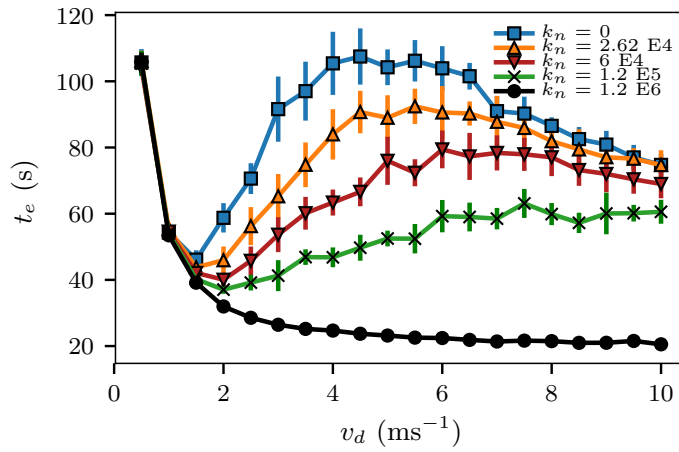
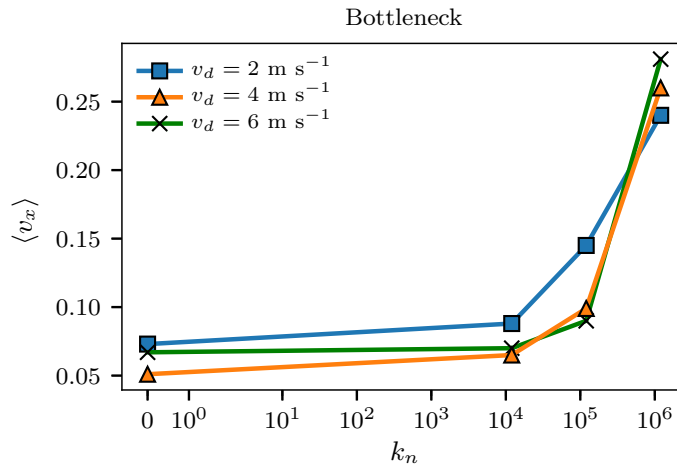


Figure 2: Mean evacuation time (s) vs. the pedestrians desired velocity (m/s) for a bottleneck. The room was 20 m x 20 m size. The door was 0.92 m width (two pedestrians' width). Mean values were computed from 10 evacuation processes. 225 pedestrians were initially placed in a square lattice with a random initial velocity. Each process was finished when 158 pedestrians left the room. The different symbols indicate the  $k_n$  value corresponding to the body force (see the label). The crosses correspond to the Helbing's original SFM parameter, the up-triangles correspond to the value measured in Ref. [37], squares correspond to zero body force and circles correspond to an extreme value of stiffness (one order of magnitude higher than the original SFM). The down triangles correspond to an intermediate value between the empirical value presented in Ref. [37] and the one provided by Helbing in Ref. [1]

ined interval). This means that stiffer pedestrians evacuate faster than soft pedestrians. To further investigate this phenomenon, we computed the mean velocity of the whole crowd as a function of the stiffness  $k_n$ . Fig. 3 shows the actual mean velocity in the  $x$ -direction as a function of the stiffness  $k_n$  for three different desired velocities. In all cases, the velocity increases with the stiffness. The most significant increment of velocity is in the interval  $k_n > 10^4$ .



(a)

Figure 3: Mean velocity in the  $x$ -direction as a function of the stiffness level  $k_n$  for different desired velocities (see label). The data corresponds to a bottleneck with periodic boundary conditions (re-injecting pedestrians). The average was taken every five seconds once the crowd reaches the stationary state ( $t = 20$  s) until the end of the simulation ( $t = 1000$  s). Color online only.

The existence of the FIF phenomenon for only “stiff” individuals opens many questions on the microscopic dynamics of pedestrians. We may presume that contacts between pedestrians are quite different for soft individuals than for stiff individuals. Thus, we proceed to study the dynamics of contacting pedestrians, regardless of the overlap effects. We will assimilate the pedestrians as nodes and the whole crowd as a network. We will link any two individuals whenever they get in physical contact (*i.e.*  $r_{ij} \leq R_{ij}$ ).

Fig. 4a shows the mean degree of the contact network as a function of the

desired velocity. The degree of a node is defined as the number of links that connects this node to any other node. This means, the number of pedestrians that are in physical contact with a given pedestrian. The mean degree is the average of the degree over all the nodes (pedestrians) and over the whole sampled interval. We computed mean values only after the system reached the stationary state, that is, after a well-formed bulk has been established.

Notice that the mean degree increases as  $v_d$  increases, as expected. This expresses the fact that higher  $v_d$  values accomplish higher densities, forcing individuals to touch each other. For a given  $v_d$ , the mean degree reduces as the  $k_n$  value increases. A noticeable decrease in the mean degree can be seen for the highest explored value of  $k_n$ . This opens the question on how would this affect the sliding friction among pedestrians.

A more detailed insight into the contact dynamics can be acquired from Fig. 4b. The overlap between individuals is shown as a function of  $v_d$ . Recall from Section 3.1 that the overlap is defined as  $R_{ij} - r_{ij}$  where  $R_{ij}$ , is the sum of radius of particle  $i$  and particle  $j$  and  $r_{ij}$  is the distance between both particles. Except for very low desired velocities (say,  $v_d < 2$  m/s), we can see that the mean overlap is an increasing function of  $v_d$  (withing the studied range of  $v_d$  and  $k_n$ ).

The regime for  $v_d < 2$  m/s is qualitatively different from the clogged regime since most of the pedestrians are not touching each other (as was already observed in Ref [2, 4]). The only pedestrians who touch each other are the ones who are being re-injected on the opposite side of the room. These collide with the bulk, providing some kind of overlap during very short time. We will not analyze this regime.

Besides, for a given  $v_d > 2$  m/s, the overlap increases as the  $k_n$  value decreases. This can be explained by considering the bulk at a (quasi) equilibrium situation. The social and compression forces counterbalance the desired force. Thus, for any fixed  $v_d$ , the product  $k_n \times (R_{ij} - r_{ij})$  remains (almost) fixed. Any decrease in  $k_n$  allows a more significant intrusion. This (partially) supports the argument that the sliding friction should weaken for stiffer pedestrians (say increasing  $k_n$  values).

The sliding friction reduction appears as the first feature for enhancing



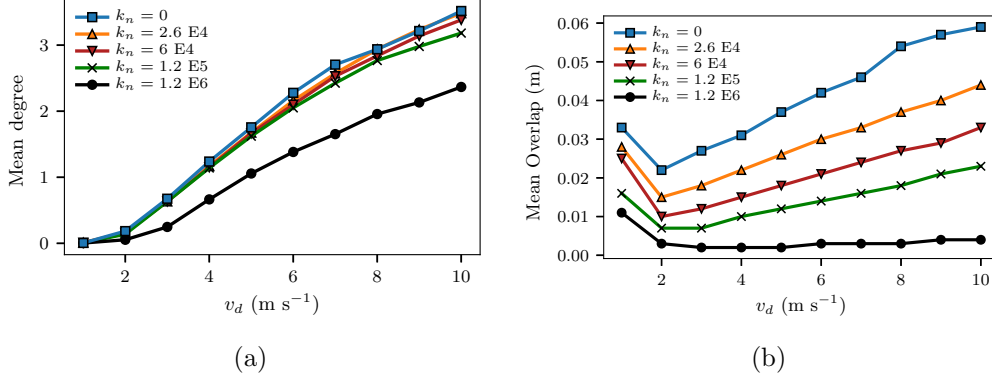


Figure 4: (a) Mean degree as a function of the pedestrians desired velocity. (b) Mean overlap as a function of the pedestrians desired velocity. Each symbol indicates the  $k_n$  value corresponding to the body force (see the labels). The data corresponds to a bottleneck with periodic boundary conditions (re-injecting pedestrians). The average was taken over time and the pedestrians in the bottleneck. The sampling was done every five seconds once the crowd reached the stationary state (say,  $t = 20$  s) until the end of the simulation ( $t = 1000$  s). Color online only.

the overall evacuation performance. Either reducing the mean overlap and the mean degree tend to diminish the mean sliding friction within the crowd. Notice, however, that switching from a FIS regime (positive slope) to a FIF regime (negative slope) in Fig. 2 appears as a more complex phenomenon. We will focus on this issue in an upcoming investigation.

The body force has a notorious impact in the number of pedestrians touching each other (say, the degree). This is clearly depicted in Fig. 5 where four different configurations of the evacuation dynamics are shown. The configurations represent 225 pedestrians trying to escape through a door (see caption for details). The colors correspond to the degree of each node (pedestrian), and the lines between pedestrians represent the contacts among them.

The four configurations corresponds to two different  $v_d$  and two different  $k_n$  values (say, the minimum and maximum explored values). Fig. 5a and Fig. 5b show snapshots for  $k_n = 0$ , at the desired velocities of 2 m/s and 10 m/s, respectively. Fig. 5c and Fig. 5d show similar situations, but for  $k_n = 1.2 \text{ E}6$ . As expected, increasing the desired velocity compresses the crowd towards the exit.

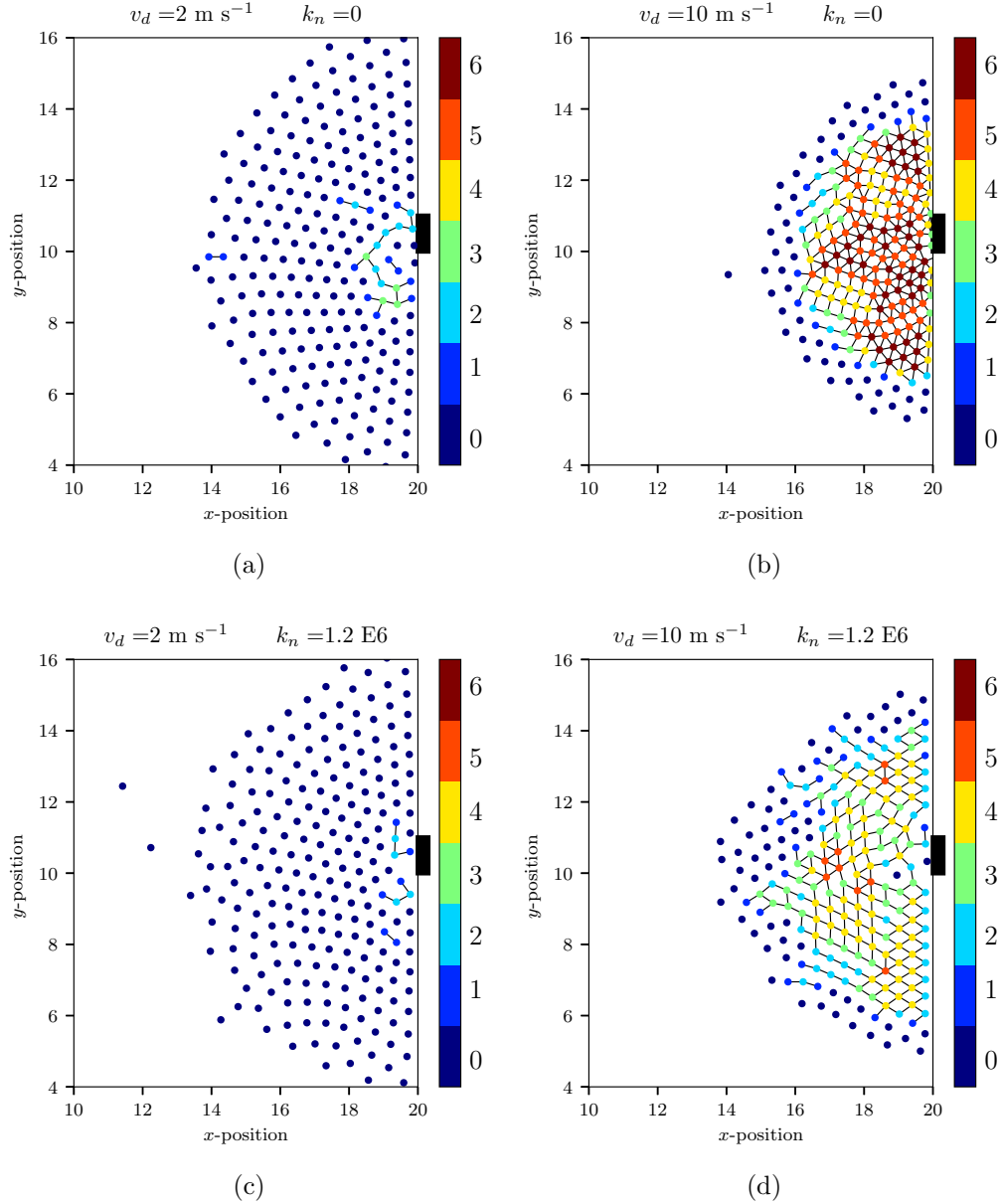


Figure 5: Snapshots of the contact networks of a 225 pedestrian evacuation through a bottleneck. The door is placed at  $(x, y) = (20, 10)$  m, the width of the door is 0.92 m (equivalent to 2 pedestrian's diameter). The lines that connect the nodes (pedestrians) represent the contact between them. The color represents the degree (the number of pedestrians with which it is connected). (a) and (b) correspond to a simulation without body force with  $v_d = 2$  and  $v_d = 10$  respectively. (c) and (d) correspond to simulations with  $k_n = 1.2 \text{ E}6$  with  $v_d = 2$  and  $v_d = 10$  respectively. The black rectangle at the right represents the exit door. Color online only. <sup>18</sup>

The four snapshots in Fig. 5 confirm (visually) the fact that more rigid pedestrians ease the crowded environment, widening the occupied region. At  $v_d = 10$  m/s (the maximum explored velocity), it can hardly be found pedestrians with degree 6 when  $k_n = 1.2 \text{E}6$ , while a lot of them are present for  $k_n=0$ .

The clusterization of the pedestrians has a significant impact on the blocking clusters (the group of pedestrians that clog the exit). Fig. 6 shows the blocking cluster probability as a function of the desired velocity for different  $k_n$  values (see caption for details). The blocking clusters become more probable for high desired velocity, since the clogged area gets more compact as  $v_d$  increases (for any fixed value of  $k_n$ ). But, the most remarkable fact in Fig. 6 is that increasing the body stiffness reduces the blocking cluster probability for any fixed value of  $v_d$ . Recall from Ref. [2] that the evacuation time is controlled by the blocking. Thus, increasing the body stiffness affects the presence of the blocking clusters, and consequently improves the evacuation time. This raises as a second feature for enhancing the overall evacuation performance.

We may summarize this Section as follows. We explored the parameter space along  $v_d$  and  $k_n$  for the bottleneck situation. This is similar to explore the dimensionless plane  $(\mathcal{A}, \mathcal{K}_c)$ . Soft pedestrians attain a FIS or FIS+FIF evacuation pattern but, stiff pedestrians (for any fixed  $\mathcal{A}$  value within the explored range) exhibit a single FIF pattern. Stiffness affects either the presence of the blocking clusters and the pedestrians overlap. The less they overlap, the less intense becomes the sliding friction among them. Additionally, the fewer the blocking clusters the easier they get out.

## 5.2. Corridor

We present in this section the results corresponding to the corridor geometry. We show the effects of varying the body force coefficient  $k_n$  on the collective dynamics. We will keep  $v_d$  (or  $\mathcal{A}$ ) fixed along this Section.

We first computed the contact network in the same way as in the bottleneck geometry. Fig. 7a shows the mean degree as a function of the global

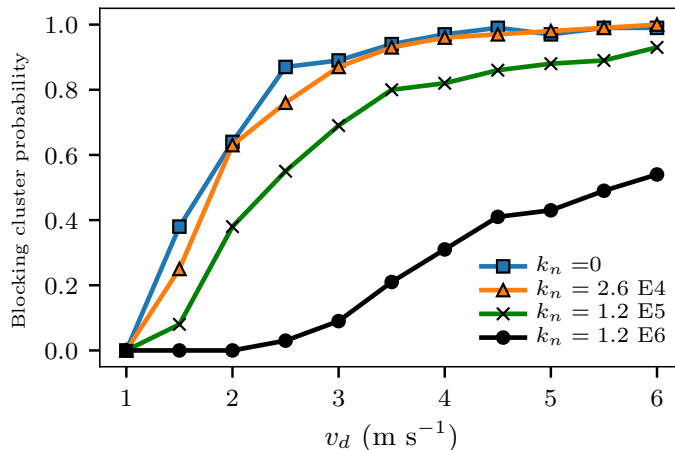


Figure 6: Blocking cluster probability as a function of  $v_d$  for different stiffness levels (see label). The probability is calculated as the amount of time a blocking cluster is present divided by the overall simulation time. The situation corresponds to a bottleneck with 225 pedestrians under periodic boundary conditions (re-injection of pedestrians once they left the room). The sampled interval was set to  $t_f = 1000$  s. Color online only.

density for different  $k_n$  values (see caption for details). The mean degree vanishes at very low densities because the pedestrians do not touch each other. When the density surpasses 4.5, a few pedestrians start to touch each other, raising the mean degree. As the density continuous increasing, the mean degree approaches the asymptotic value of six. Degree six corresponds to the maximum packing density for identical hard disks.

It is worth noting from Fig. 7a that “stiff” pedestrians exhibit a sharper transition to the maximum packing density than the “soft” pedestrians. We further checked this phenomenon by counting the number of loops of three nodes (say, the triangles) present in the network. This magnitude was reported to be a sensitive magnitude for characterizing the jamming transition in a compressed granular packing (see Ref. [36] for details). As can be seen in Fig. 7b, the “stiff” pedestrians share more triangles than the “soft” ones.

In order to get a better insight on how the pedestrians contact to each other, we present in Fig. 8 two snapshots of the corridor at the stationary situation. Fig. 8a corresponds to  $k_n = 0$ , while Fig. 8b corresponds to

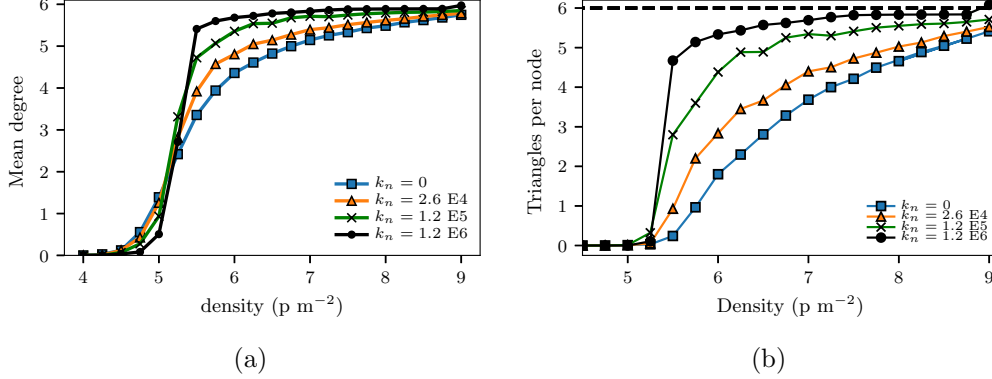


Figure 7: (a) Mean degree as a function of the global density for different  $k_n$  values. (b) Triangles per node as a function of the global density. The global density is the total number of pedestrians per unit area. The mean values are averages over all the pedestrians and over time once the system reached the stationary state. The measurements correspond to a corridor of  $28 \text{ m} \times 22 \text{ m}$  with periodic boundary conditions and  $v_d = 1$ . Color online only.

$k_n = 1.2 \text{ E}5$ . The former shows a somewhat disordered network, while the latter exhibits an almost completely ordered lattice. The missing triangles in Fig. 8a are replaced by other polygons of more than three edges.

We find these topological magnitudes useful for comparing the pedestrian behavior in the corridor geometry with respect to the bottleneck geometry. A re-examination of Fig. 7a (corridor) and Fig. 4a (bottleneck) reveal that the pedestrian stiffness  $k_n$  affects differently the way they contact each other. The mean degree increases for “stiff” pedestrians moving along the corridor as the density increased with a sharp increase at  $5 \text{ p/m}^2$ . Conversely, the mean degree increases for “soft” pedestrians in the bottleneck situation.

Fig. 5 and Fig. 8 illustrate the connectivity differences between the bottleneck and the corridor situation. The bulk in Fig. 5 appears more heavily connected among “soft” pedestrians than among “stiff” pedestrians (see both snapshots at  $v_d = 10$ ). The opposite occurs in Fig. 8. This discrepancy seems to be related to the boundary conditions, since the same SFM parameters were applied on both situations. We may speculate that this phenomenon occurs because, in the corridor, the lateral walls act like a confining barrier

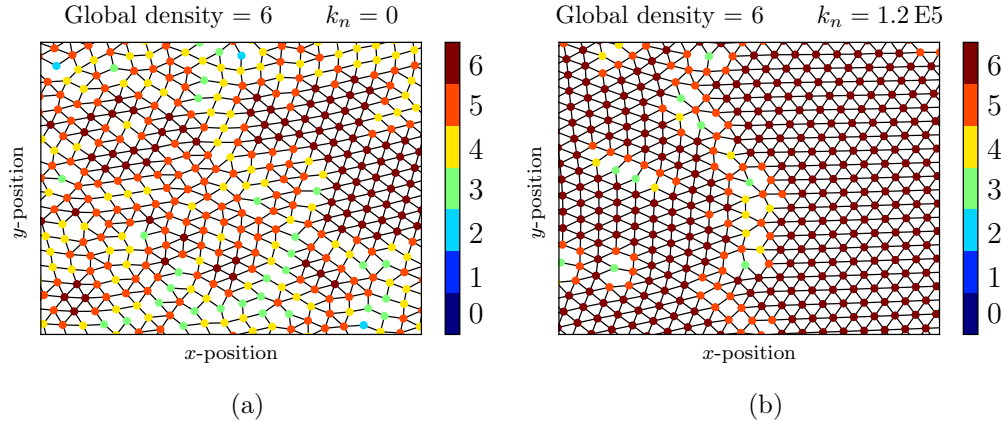


Figure 8: Contact network of the pedestrians along the corridor at time  $t = 50$ s. The global density was  $\rho = 6$ . The lines that connect the nodes (pedestrians) represent the contacts between them. The colors stand for the degree of the node (the number of pedestrians that are in contact with him/her). The corridor was  $28 \text{ m} \times 22 \text{ m}$  with periodic boundary conditions and  $v_d = 1$ . (a) corresponds to a simulation without body force and (b) corresponds to a simulation with  $k_n = 1.2 \text{ E}5$ . The friction coefficient and the other SFM parameters are the same as in Section 5.1. Color online only.

that forces the “stiff” pedestrian to increase his (her) contacts. On the contrary, no real confining walls exist in the bottleneck situation (regardless the side walls).

We can test our hypothesis by computing the mean overlap. Fig. 9 shows this magnitude for the corridor situation. Notice that “soft” pedestrians attain more overlap than the “stiff” ones, as expected. This is in agreement with Fig. 4b for the bottleneck situation (at a fixed value of  $v_d$ ). The curves in Fig. 4b, however, do not meet each other as in Fig. 9 where all the curves meet each other at high-density values. This phenomenon occurs due to space limitations in the corridor that produces overlapping (almost) independently of the value of  $k_n$ .

The above results represent an important step in the investigation. The inter-pedestrian connectivity differences between the bottleneck geometry and the corridor geometry were not expected and opens two major questions: how do the pedestrians interact with the walls as a function of the body stiffness, and consequently, how does this affect the flux across the cor-

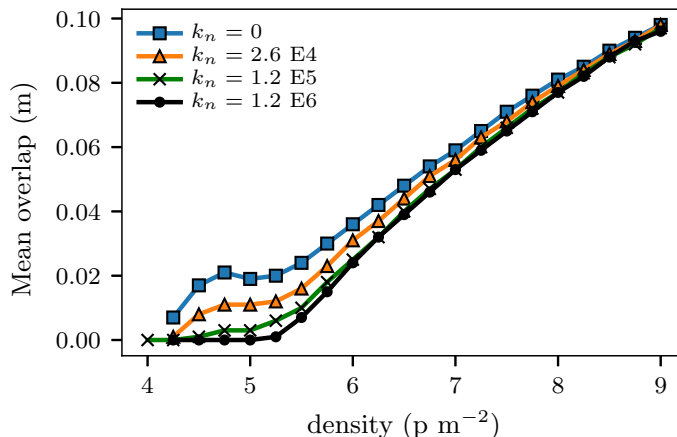


Figure 9: Mean overlap as a function of the global density. The global density is the total number of pedestrians per unit area. The mean values are averages over all the pedestrians and over time once the system reached the stationary state. Both measurements correspond to the corridor geometry with desired velocity  $v_d = 1$ . Color online only.

ridor.

We start by computing the mean velocity across the corridor. Fig. 10 shows the mean velocity  $\langle v_x \rangle$  (parallel to the corridor) as a function of the stiffness for different global density levels. This plot shows a flat pattern for  $k_n < 10^4$  and a slowing down above this threshold. Notice from Fig. 3 that this is opposed to what happens in the bottleneck geometry.

The  $\langle v_x \rangle$  values in Fig. 10 were computed at densities  $\rho \geq 5.5$ . According to Fig. 9, at these densities, the overlaps among pedestrians attain significant values. Furthermore, stiffness values  $k_n \geq 10^4$  move the system to a more heavily connected stage, and thus, pedestrians have no choice but to walk at (almost) the same speed as his (her) neighbors. This behavior may be envisaged as the passage from a “free” walking movement to a constrained walking movement as the stiffness increases. A more physical picture would assimilate the former as a “fluid-like state” and the latter as a “solid-like state”. When the stiffness is very high (say  $k_n = 1.2 \text{ E6}$ ), all the pedestrians are expected to walk at a common velocity. The pedestrians that walk in physical contact with the wall are the ones who determine the velocity of the

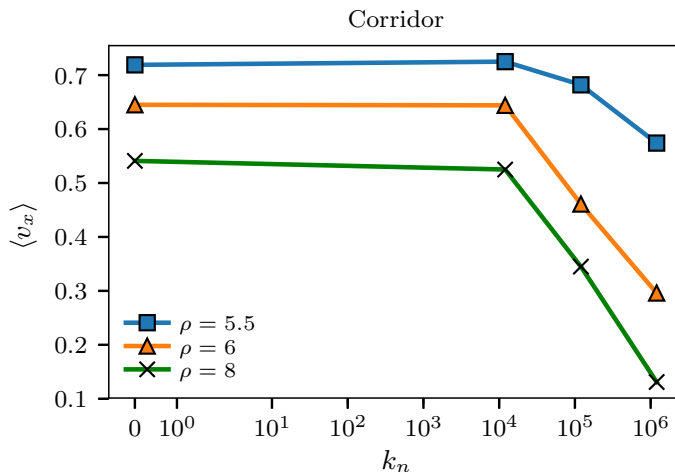


Figure 10: Mean velocity in the longitudinal coordinate ( $v_x$ ) as a function of the stiffness  $k_n$  for three different global densities (see label in the plot). The measurements correspond to a corridor of  $28 \text{ m} \times 22 \text{ m}$  with periodic boundary conditions and  $v_d = 1$ . The average was taken along the corridor and along the simulated time. Color online only.

whole crowd, as discussed below.

Fig. 11a shows the velocity profile ( $\langle v_x \rangle$  vs. the transversal coordinate  $y$ ) for different  $k_n$  values. For  $k_n = 0$ , we can see a parabolic-like velocity profile which means that the friction with the walls reduces the speed of pedestrians. The velocity profile resembles the Poiseuille flow (similar to Newtonian and incompressible fluids in a laminar regime). This behavior was also observed in empirical measurements of crowd dynamics reported in Ref. [38]. But as  $k_n$  increases the velocity profile flattens until becoming (almost) uniform (see Fig. 11a for  $k_n = 1.2 \text{ E}6$ ). In this scenario,  $v_x$  attains a much lower value than in the case of soft pedestrians ( $k_n = 0$ ).

From the results displayed above, we realize that the crowd behaves like a solid for very stiff pedestrians. This means that the crowd can not be easily “deformed”. In this context, deformation means that some parts of the crowd may be allowed to move faster than other parts of the crowd.

The strain rate tensor displays the rate of change of the deformation of a body in the vicinity of a given point. We consider the following discrete



definition of the strain rate:

$$\dot{\gamma} = \frac{\langle v_x(\text{center}) \rangle - \langle v_x(\text{boundary}) \rangle}{|y(\text{center}) - y(\text{boundary})|} \quad (6)$$

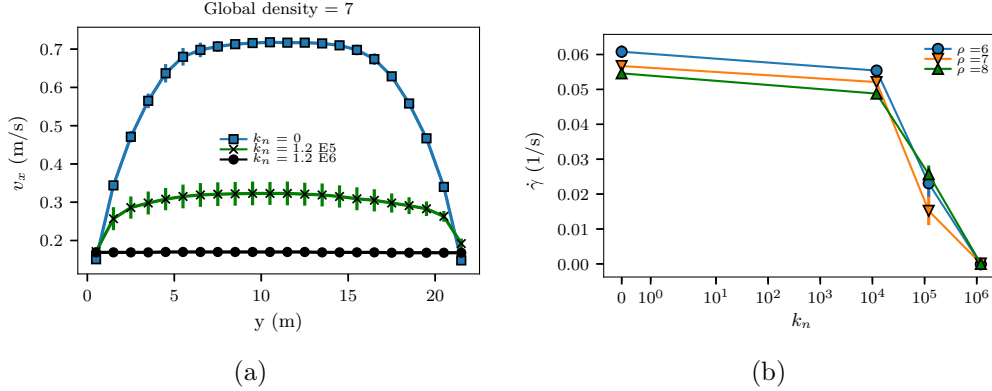


Figure 11: (a) Mean velocity in the  $x$  coordinate as a function of the transversal coordinate  $y$  for three different stiffness values  $k_n$  (see the label). (b) Strain rate as a function of the stiffness level  $k_n$  for three different global density values (see label). Data correspond to a corridor of  $28 \text{ m} \times 22 \text{ m}$  with periodic boundary conditions and  $v_d = 1$ . The global density was  $\rho = 7 \text{ p m}^{-2}$ . Color online only.

Where  $\langle \cdot \rangle$  means the average taken over time. This definition compares the velocity of the pedestrians close to the wall (boundary) with respect to the velocity of the pedestrians at the center of the corridor (center). Thus, the strain rate  $\dot{\gamma}$  vanishes (no deformation) as the stiffness level increases. This phenomenon is shown in Fig. 11b where we can see that the strain rate drops for high values of  $k_n$ .

We conclude this Section by stressing, once again, that stiffer pedestrians attain opposite results in corridors with respect to bottlenecks. The walls in the corridors play a critical role that prevents pedestrians from detaching from each other. This effect can be observed as an increment in the connectivity of the contact network and the flattening of the velocity profile (thus reducing the strain rate). High enough stiffness values stuck the pedestrians leading to a “solidification” of the crowd. All the pedestrians walk at almost the same velocity at this stage. The pedestrians that are in contact with the walls are the ones that determine the velocity of the whole crowd. We

already analyzed this situation in Ref [20].

### 5.3. Dimensionless numbers and comparison with empirical data

The final stage of our investigation deals with the plausible values of the dimensionless numbers  $\mathcal{K}_c$  and  $\mathcal{K}$ , in comparison to the empirical measurements. We vary the body force coefficient ( $k_n$ ) and the friction coefficient ( $k_t$ ) to explore different values of  $\mathcal{K}_c$  and  $\mathcal{K}$ , respectively.

We consider the empirical measurements from Ref. [23] corresponding to the fundamental diagram obtained at the entrance of the Jamaraat bridge (see the inset in Fig. 12a). Our aim is to reproduce the qualitative behavior of these measurements.

Figs. 12 show the pedestrian flow as a function of the global density (fundamental diagram). Fig. 12a corresponds to  $\mathcal{K}_c = 0$  (this is *i.e.*  $k_n = 0$ ) while Fig. 12b corresponds to  $\mathcal{K}_c = 68$  corresponding to the original SFM with  $k_n = 1.2 \text{E}5$ . Each curve represents different friction values (see the caption for details).

According to the empirical measurements at Jamaraat, the flow slows down for high enough densities due to jamming. Notice that the original SFM (corresponding to  $\mathcal{K} = 137$ ) does not produce the expected slowing down for null body force ( $\mathcal{K}_c = 0$ ). However, when the body force is present (the original SFM) an “U” shape behavior occurs for densities above  $5 \text{ p}^{-2}$ .

The increase in  $\mathcal{K}$  to  $\mathcal{K} = 685$  (five times the original SFM value) slows down the flux for densities above  $5 \text{ p m}^{-2}$ , regardless of the presence of the body force. Including the body force, however, produces a subtle increment in the flow for densities higher than  $7 \text{ p m}^{-2}$  (see orange curve from Fig. 12a).

A further increment of  $\mathcal{K}$  to  $\mathcal{K} = 1371$  (ten times the original SFM value) attains a plateau ( $\rho > 5 \text{ p m}^{-2}$ ) before vanishing at very high densities. This occurs on either  $\mathcal{K}_c = 0$  and  $\mathcal{K}_c = 68$ .

These results suggest that although increasing  $\mathcal{K}_c$  slows down the flux, it is still necessary to increase  $\mathcal{K}$  (by increasing the friction coefficient  $k_t$ ) to avoid an “U” shape behavior for extremely high densities. It is still a

challenge to find the optimal dimensionless numbers ( $\mathcal{A}, \mathcal{K}, \mathcal{K}_c$ ) for the fundamental diagram. Our inspection into the parameter set is a first approach to narrow down the search.

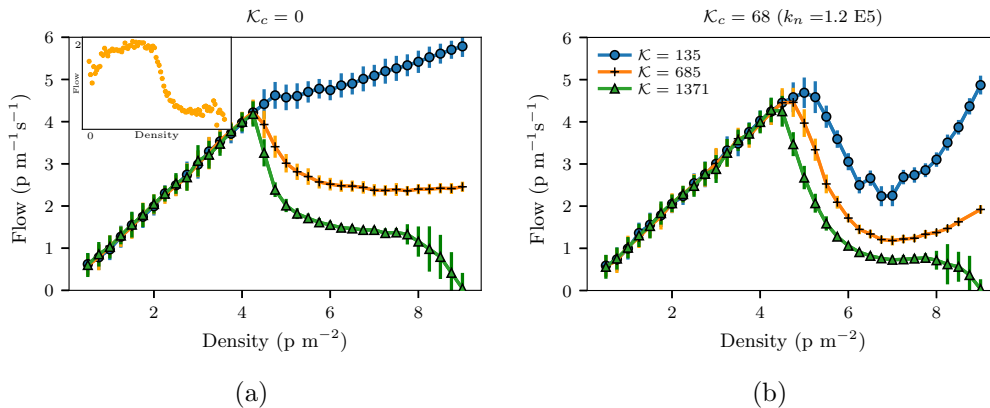


Figure 12: Flow vs. global density. The flow is calculated in a circular area of  $R = 1$  m at the center of the corridor. The circular markers correspond to the original friction of the SFM, the "+" symbol corresponds to the friction increased by a factor of five and the triangles correspond to the friction increased by a factor of ten. The desired velocity was  $v_d = 1$  in all the cases. (a) corresponds to simulations without body force ( $\mathcal{K}_c = 0$ ) and (b) corresponds to a body force with the original value of the body stiffness ( $\mathcal{K}_c = 68$ ). Color online only.

## 6. Conclusions

Having adopted as fundamental philosophy of work that the parameters of the SFM should be properly determined by requiring that the model reproduces well established experimental data; we explored the effect on the pedestrians dynamics of the (sometimes neglected) body force in the framework of the SFM. We showed that the stiffness coefficient ( $k_n$ ) has a significant impact on the evacuation dynamics (bottleneck) and also in the dynamics of pedestrians walking along a straight corridor.

In the bottleneck geometry, the evacuation time diminishes (pedestrians move faster) as pedestrians become stiffer along the explored desired velocities. This phenomenon occurs because stiffer pedestrians reduce the

overlapping and hence the sliding friction intensity. This scenario releases more easily the pedestrians and reduces the probability of producing a cluster of pedestrians blocking the exit (blocking cluster). This leads to a more efficient evacuation dynamics.

The opposite behavior is obtained in the corridor geometry with respect to the bottleneck geometry. The major difference is that pedestrians are limited to the available space between walls in the corridor geometry. Walls are not relevant in the bottleneck geometry. Thus, the overlap between pedestrians is controlled by the available space. But, stiffer pedestrians are more likely to get stuck. The whole crowd can be compared to a granular material. Granular materials can be disordered (amorphous) or ordered depending on how particles interact with each other. In the present context, at low stiffness levels, the crowd appears disordered attaining a parabolic velocity profile. If the stiffness level is high, the whole crowd appears ordered into a lattice (like a crystalline solid) with a uniform velocity profile that depends on the friction interaction with the walls.

Our efforts to “tune” the original SFM to reproduce empirical data (say, the fundamental diagram) moved us to explore the dimensionless parameter space. We found that we can qualitatively reproduce the empirical data if the parameters are close to  $\mathcal{K}_c < 68$ ,  $\mathcal{K} = 685$  and  $\mathcal{A} = 14$ . Nevertheless, this is a first attempt to arrive at suitable parameters, although we do not claim these to be optimal. We encourage further research to find dimensionless numbers that may better fit experimental data.

## Acknowledgments

This work was supported by the National Scientific and Technical Research Council (spanish: Consejo Nacional de Investigaciones Científicas y Técnicas - CONICET, Argentina) grant Programación Científica 2018 (UBA-CYT) Number 20020170100628BA.

The authors want to thank the degree students Josefina Catoni and Ayeleen Santos for providing data acquired at the subway in Buenos Aires, Argentina.

G. Frank thanks Universidad Tecnológica Nacional (UTN) for partial support through Grant PID Number SIUTNBA0006595.

## Appendix A. Reduced-in-units equation of motion

The SFM description in section 3.1 introduces seven parameters ( $m$ ,  $\tau$ ,  $v_d$ ,  $B$ ,  $A$ ,  $k_t$  and  $k_n$ ) attaining for the “individual” behavior of each pedestrian. The collective dynamic, however, requires a smaller set of parameters. In order to identify this smaller set, we introduce the following dimensionless magnitudes

$$\begin{cases} t' &= t/\tau \\ r' &= r/B \\ v' &= v/v_d \end{cases} \quad (\text{A.1})$$

The equation of motion (1) can be rewritten in terms of these (dimensionless) magnitudes, while only three (reduced) parameters are needed.

$$\frac{d\mathbf{v}'}{dt'} = \hat{\mathbf{e}}_d - \mathbf{v}' + \mathcal{A} e^{R'-r'} \hat{\mathbf{n}} + g(R' - r') \left[ \mathcal{K} (\Delta\mathbf{v}' \cdot \hat{\mathbf{t}}) \hat{\mathbf{t}} + \mathcal{K}_c \hat{\mathbf{n}} \right] \quad (\text{A.2})$$

where the smaller set  $(\mathcal{A}, \mathcal{K}, \mathcal{K}_c)$  means

$$\mathcal{A} = \frac{A\tau}{m v_d} \quad , \quad \mathcal{K} = \frac{k_t B \tau}{m} \quad , \quad \mathcal{K}_c = \frac{k_n B \tau}{m v_d} \quad (\text{A.3})$$

Notice that the SFM will arrive to similar collective dynamics whenever the reduced set  $(\mathcal{A}, \mathcal{K}, \mathcal{K}_c)$  remains unchanged (although some “individual” parameters are allowed to change). For a deep explanation on the meaning of the set  $(\mathcal{A}, \mathcal{K}, \mathcal{K}_c)$  see section 3.2.

## References

- [1] D. Helbing, I. Farkas, and T. Vicsek. Simulating dynamical features of escape panic. *Nature*, 407:487–490, 2000.

- [2] D. Parisi and C. Dorso. Microscopic dynamics of pedestrian evacuation. Physica A, 354:606–618, 2005.
- [3] D. Parisi and C. Dorso. Morphological and dynamical aspects of the room evacuation process. Physica A, 385:343–355, 2007.
- [4] G. Frank and C. Dorso. Room evacuation in the presence of an obstacle. Physica A, 390:2135–2145, 2011.
- [5] Colin M. Henein and Tony White. Macroscopic effects of microscopic forces between agents in crowd models. Physica A: Statistical Mechanics and its Applications, 373:694 – 712, 2007.
- [6] J. Fruin. The causes and prevention of crowd disasters. In R.A. Smith and J.F. Dickie, editors, Engineering for Crowd Safety. Elsevier, 1993.
- [7] Taras I. Lakoba, D. J. Kaup, and Neal M. Finkelstein. Modifications of the helbing-molnr-farkas-vicsek social force model for pedestrian evolution. SIMULATION, 81(5):339–352, 2005.
- [8] Paul A. Langston, Robert Masling, and Basel N. Asmar. Crowd dynamics discrete element multi-circle model. Safety Science, 44(5):395 – 417, 2006.
- [9] Peng Lin, Jian Ma, You-Ling Si, Fan-Yu Wu, Guo-Yuan Wang, and Jian-Yu Wang. A numerical study of contact force in competitive evacuation. Chinese Physics B, 26(10):104501, sep 2017.
- [10] I. M. Sticco, F. E. Cornes, G. A. Frank, and C. O. Dorso. Beyond the faster-is-slower effect. Phys. Rev. E, 96:052303, Nov 2017.
- [11] Rahul Narain, Abhinav Golas, Sean Curtis, and Ming C. Lin. Aggregate dynamics for dense crowd simulation. ACM Trans. Graph., 28(5):122:1–122:8, December 2009.
- [12] N. Pelechano, J. Allbeck, and N. Badler. Controlling individual agents in high-density crowd simulation. Proceedings of the 2007 ACM SIGGRAPH/Eurographics Symposium on Computer Animation, pages 99–108, 2007.

- [13] Mehdi Moussaïd, Dirk Helbing, and Guy Theraulaz. How simple rules determine pedestrian behavior and crowd disasters. Proceedings of the National Academy of Sciences, 108(17):6884–6888, 2011.
- [14] Fernando Alonso-Marroquín, Jonathan Busch, Coraline Chiew, Celia Lozano, and Álvaro Ramírez-Gómez. Simulation of counterflow pedestrian dynamics using spheropolygons. Phys. Rev. E, 90:063305, Dec 2014.
- [15] Arianna Bottinelli and Jesse L. Silverberg. How to: Using mode analysis to quantify, analyze, and interpret the mechanisms of high-density collective motion. Frontiers in Applied Mathematics and Statistics, 3:26, 2017.
- [16] J. Song, F. Chen, Y. Zhu, N. Zhang, W. Liu, and K. Du. Experiment calibrated simulation modeling of crowding forces in high density crowd. IEEE Access, 7:100162–100173, 2019.
- [17] Bachar Kaban. Crowd dynamics: modeling pedestrian movement and associated generated forces. Theses, Université Paris-Est, January 2016.
- [18] A. Jebrane, P. Argoul, A. Hakim, and M. El Rhabi. Estimating contact forces and pressure in a dense crowd: Microscopic and macroscopic models. Applied Mathematical Modelling, 74:409 – 421, 2019.
- [19] Litao Wang and Shifei Shen. A pedestrian dynamics model based on heuristics considering contact force information and static friction. Transportmetrica B: Transport Dynamics, 7(1):1117–1129, 2019.
- [20] I.M. Sticco, G.A. Frank, F.E. Cornes, and C.O. Dorso. A re-examination of the role of friction in the original social force model. Safety Science, 121:42 – 53, 2020.
- [21] Yaouen Fily, Silke Henkes, and M. Cristina Marchetti. Freezing and phase separation of self-propelled disks. Soft Matter, 10:2132–2140, 2014.
- [22] Milad Haghani, Majid Sarvi, and Zahra Shahhoseini. When push does not come to shove: Revisiting faster is slower in collective egress of human crowds. Transportation Research Part A: Policy and Practice, 122:51 – 69, 2019.

- [23] Dirk Helbing, Anders Johansson, and Habib Zein Al-Abideen. Dynamics of crowd disasters: An empirical study. Phys. Rev. E, 75:046109, Apr 2007.
- [24] Rainald Lohner, Britto Muhamad, Prabhu Dambalmath, and Eberhard Haug. Fundamental diagrams for specific very high density crowds. Collective Dynamics, 2, 2018.
- [25] Dirk Helbing and Péter Molnár. Social force model for pedestrian dynamics. Phys. Rev. E, 51:4282–4286, May 1995.
- [26] Anders Johansson. Constant-net-time headway as a key mechanism behind pedestrian flow dynamics. Phys. Rev. E, 80:026120, Aug 2009.
- [27] Meifang Li, Yongxiang Zhao, Lerong He, Wenxiao Chen, and Xianfeng Xu. The parameter calibration and optimization of social force model for the real-life 2013 yaan earthquake evacuation in china. Safety Science, 79:243 – 253, 2015.
- [28] Ulrich Weidmann. Transporttechnik der fussgänger. IVT Schriftenreihe, 90, Jan 1992.
- [29] S.P. Hoogendoorn and W. Daamen. Microscopic Calibration and Validation of Pedestrian Models: Cross-Comparison of Models Using Experimental Data. In A. Schadschneider, T. Pöschel, R. Kühne, M. Schreckenberg, and D. E. Wolf, editors, Traffic and granular flow '05, volume Part III. Springer, 2007.
- [30] A. Seyfried, B. Steffen, W. Klingsch, Th. Lippert, and M. Boltes. The Fundamental Diagram of Pedestrian Movement Revisited - Empirical Results and Modelling. In A. Schadschneider, T. Pöschel, R. Kühne, M. Schreckenberg, and D. E. Wolf, editors, Traffic and granular flow '05, volume Part III. Springer, 2007.
- [31] A. Johansson, D. Helbing, and P.K. Shukla. Specification of the social force pedestrian model by evolutionary adjustment to video tracking data. Advances in Complex Systems, 10(supp02):271–288, 2007.
- [32] Mehdi Moussaï d, Dirk Helbing, Simon Garnier, Anders Johansson, Maud Combe, and Guy Theraulaz. Experimental study of the behavioural mechanisms underlying self-organization in human crowds.



Proceedings of the Royal Society B: Biological Sciences, 276(1668):2755–2762, 2009.

- [33] M. Luber, J. A. Stork, G. D. Tipaldi, and K. O. Arras. People tracking with human motion predictions from social forces. In 2010 IEEE International Conference on Robotics and Automation, pages 464–469, May 2010.
- [34] Stefan Seer, Christian Rudloff, Thomas Matyus, and Norbert Brändle. Validating social force based models with comprehensive real world motion data. Transportation Research Procedia, 2:724 – 732, 2014. The Conference on Pedestrian and Evacuation Dynamics 2014 (PED 2014), 22-24 October 2014, Delft, The Netherlands.
- [35] S. M. P. Siddharth and P. Vedagiri. Modeling the gender effects of pedestrians and calibration of the modified social force model. Transportation Research Record, 2672(31):1–9, 2018.
- [36] Arévalo, Roberto and Pugnaroni, Luis A and Zuriguel, Iker and Maza, Diego Contact network topology in tapped granular media. Physical Review E, 87(2):022203, 2013.
- [37] Melvin, John W AATD system technical characteristics, design concepts, and trauma assessment criteria. Task EF final report
- [38] Zhang, XL and Weng, WG and Yuan, HY and Chen, JG Empirical study of a unidirectional dense crowd during a real mass event Physica A: Statistical Mechanics and its Applications, 392:2781–2791, 2013.
- [39] Plimpton, Steve Fast parallel algorithms for short-range molecular dynamics Sandia National Labs,1993
- [40] Strachan, A and Dorso, CO Fragment recognition in molecular dynamics Physical Review C, 56:995, 1997.